Comprehensive multidimensional study of the self-assembly properties of a three residue substituted β^3 oligoamide

Claire Buchanan[a], Mark G Hinds[b], Ljiljana Puskar[c], Christopher J Garvey[d,e], and Adam Mechler[a]*

[a]*Department of Chemistry and Physics, Latrobe University, Bundoora, Australia.*

[b]*Bio21 Molecular Science and Biotechnology Institute, The University of Melbourne, Parkville, Australia*

[c]*Helmholtz Zentrum Berlin für Materialien und Energie GmbH, Berlin, Germany*

[d]*Lund Institute for Advanced Neutron and X-ray Science, 223 70 Lund, Sweden*

[e] *Biofilm-Research Center for Biointerfaces and Biomedical Science Department, Faculty of Health and Society, MalmoUniversity, 211 19 Malmo, Sweden.*

Abstract: Substituted β^3 oligoamides form a unique self-assembling system where each monomer folds into a helix containing approximately three β^3 amino acids per turn, yielding a geometrically well-defined cylindrical building block that, when N-acylated, is able to self-assemble head-to-tail into nanorods that can reach several 100 μm length. It was shown in previous works that self-assembly can be achieved with a three residue long oligoamide as well that lacks any intramolecular H-bonds, yet it crystallizes in a helix-like conformation. The self-assembly properties of these small oligoamides are however elusive, suggesting a more complex system than the self-assembly of the H-bond stabilized helical monomers. Here we focus on the self-assembly behaviour of a three residue oligoamide, Ac-β^3[LIA] where the letters denote the side chain of the analogous α amino acid. Ac-β^3[LIA] can yield highly inhomogeneous suspensions in water with a broad range of large fibrous structures that seem to be very stable, yet occasionally fibre growth is only observed upon heating. The small size of the monomer suggests a highly dynamic equilibrium yet all previous attempts failed to clearly identify low molecular weight species. Therefore a special methodology was employed in this study to characterize the suspensions at different size ranges: SANS that is optimal to measure the small oligomers and cross sectional diameter of the assemblies, DLS that is sensitive to the large populations and therefore the length of the superstructures, and NMR that is sensitive to monomeric and small oligomeric form, in conjunction with IR spectroscopy to probe the folding and AFM to image the morphology of the assemblies. Temperature ramping was used to perturb the system to probe the dynamicity of the self-assembly. It was found that the anomalous self-assembly behaviour of Ac-β^3[LIA] is caused by its two stable conformations, a helix-building "horseshoe" fold and a linear conformer. The latter is exclusively found in monomeric form in solution whereas the horseshoe fold is stable in solid phase and in fibrous assemblies. Small oligomers were absent. Thus the self-assembly of Ac-β^3[LIA] is arrested by the activation energy need of the conformation change; fibre growth might be triggered by conditions that allow increased conformational freedom of the monomers. This observation may be used to develop strategies for controlled switchable self-assembly.

Keywords: spontaneous assembly, substituted oligoamides, 14-helix, temperature, β^3 peptides

1. Introduction

Substituted oligoamides are building blocks that form hierarchical nanostructured materials via supramolecular self-assembly[1-3]. As analogues of natural peptides, they are comprised of β^3 amino acids linked via amide bonds[4, 5]. β^3 amino acids differ from natural amino acids by an extra methylene group in the carbon backbone[6, 7]. If the side chains are identical to those of α amino acids, the corresponding β^3 amino acids can be described using standard peptide nomenclature. Substituted oligoamides form a highly regular, stable, and unique 14-helical secondary structure, named after the 14 atoms present in one complete loop of the helix, which is held together by a 3-point hydrogen bond motif between amide moieties at residues *i* – *i+3*, or every fourth residue in the sequence[8-10](Fig. 1). A truly unique aspect of the 14 helix is the 3-3.1 residue pitch (height of 1 complete helical loop), which results in near perfect line up of every fourth side chain to form distinct "faces" of the molecule[2, 7, 11, 12] (Fig. 1). The strength of the 14-helix fold is such that it is stable in oligoamides with as few as 4 residues[13]. When acetylated at the N-terminus, this motif can

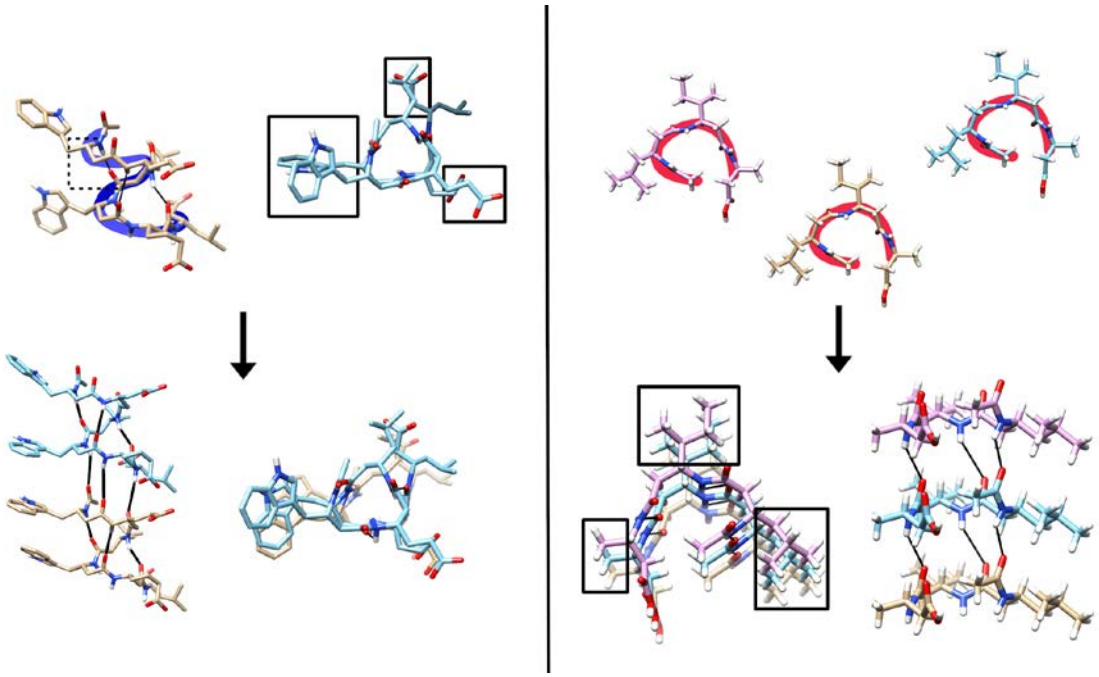

Figure 1. Schematic of monomeric and head-to-tail assembled nanorods of Ac-β^3[WELWEL] (left) and Ac-β^3[LIA] (right). Ac-β^3[WELWEL] monomer exists as a 14 helical structure (top left), with core helical structure emphasized in blue, pitch of the helix shown with dashed line, and aligned "faces" of the helix outlined with solid lines. Bottom left shows H-bonds between two Ac-β^3[WELWEL] monomers when assembled in the head to tail fashion; addition of further monomers yields nanorods. Ac-β^3[LIA] exists as an incomplete loop of the 14-helix, taht can be visualized as a "horseshoe" confirmation (top right, highlighted in red); these monomers stack together to form a nanorod similar to the 14 helix monomers, and this assembly also results in aligned sidechain "faces" (bottom right, highlighted with solid lines).

be extended to intramolecular nanorod assembly *via* head to tail assembly[14, 15] (Fig. 1). Three residue oligoamides, which have insufficient length to form a complete helical loop, have been found to form stable "horseshoe" shapes that have similar steric angle to the 14-helix[15-19] (Fig. 1). Furthermore, the oligoamide Ac-β^3[LIA] was confirmed to form fibrous assemblies due to stacking of these "horseshoe" shapes via the same H-bond motif that promotes 14-helix head to tail assembly[16].

These nanorods further assemble *via* lateral interactions such as van der Waals effects, H-bonding, π-stacking, and solvopobhic effects, governed by the physicochemical properties of the sidechains and the primary structure of the substituted oligoamides[17-19]. The final superstructures are highly dependent on both the physicochemical properties of the side chains, and the environmental factors such as solvent polarity and dielectric properties, interaction with metal ions and between different oligoamides to co-assemble[20-23]. Self-assembled structures of a wide range of β^3 oligoamides were studied, focusing on the effect of environment as well as composition and length of the sequence[13, 16-23]. It was noted that in almost all cases, large fibrous structures form, with an apparent absence of small oligomeric, or even monomeric materials[15-18]. This was particularly prominent with Ac-β^3[LIA] and its isomers, where the smallest observed fibre diameters were in the order of 10 nm, which is over 20 times larger than the expected 0.5 nm diameter of the core nanorod that was successfully identified in case of the assembly of larger oligoamides[16-18]. Ac-β^3[LIA] also exhibited inconsistent behaviour, with apparent low aqueous solubility at room temperature but a sudden formation of a visible fibre mesh at 75°C[18].

Self-assembly is an equilibrium process[13, 17, 21], and as such it should be controllable using Le Chatelier's principle. Yet, these oligoamides have proven to be highly stable and resistant to any perturbations such as dilutions or adjustment of interaction strength with solvent effects[17]. This may indicate an Ostwald ripening-like process where a complex dynamic equilibrium exists between assemblies of different size, and perturbation of the system may initiate a complex response where the new equilibrium is reached through transient intermediates. The possibility of such a system, and the apparent absence of any small species necessitates an unorthodox multifaceted approach to characterize the range of structures formed by the dynamic system, using complementary methods that cover different size ranges. The aim of this study is to use determine the effect that temperature has on the assembly of the oligoamide structures at both the monomer and supramolecular

superstructure level. Thus, we use nuclear magnetic resonance (NMR) that is sensitive to monomers and small oligomers, small angle neutron scattering (SANS) that can be used to measure the cross sectional diameter of the fibres, and dynamic light scattering (DLS) that is sensitive principally to large structures, i.e. the length of fibres in case of fibrous assembly. To trigger changes in the system and confirm the existence of a dynamic equilibrium, temperature ramping was applied to NMR, SANS, and DLS measurements. These measurements were supplemented by morphological analysis via atomic force microscopy (AFM) and structural analysis using infrared (IR) spectroscopy. The results indicate that, while there is a monomeric population of Ac-β^3[LIA] in solution, small oligomers/short fibres are not detected, only very large, GDa range assemblies consistent with extensive bundling of Ac-β^3[LIA] nanorods. The absence of small oligomers suggests that the self-assembly of Ac-β^3[LIA] is nucleation-limited, consistent with the rotational freedom of the C^2-C^3 bond [2] that in monomeric form prefers trans, i.e. fully extended conformation according to NMR, whereas the helical form requires a gauche conformation to yield the "horseshoe" fold. Thus the two conformers of Ac-β^3[LIA] have fundamentally different affinities to join a growing fibre.

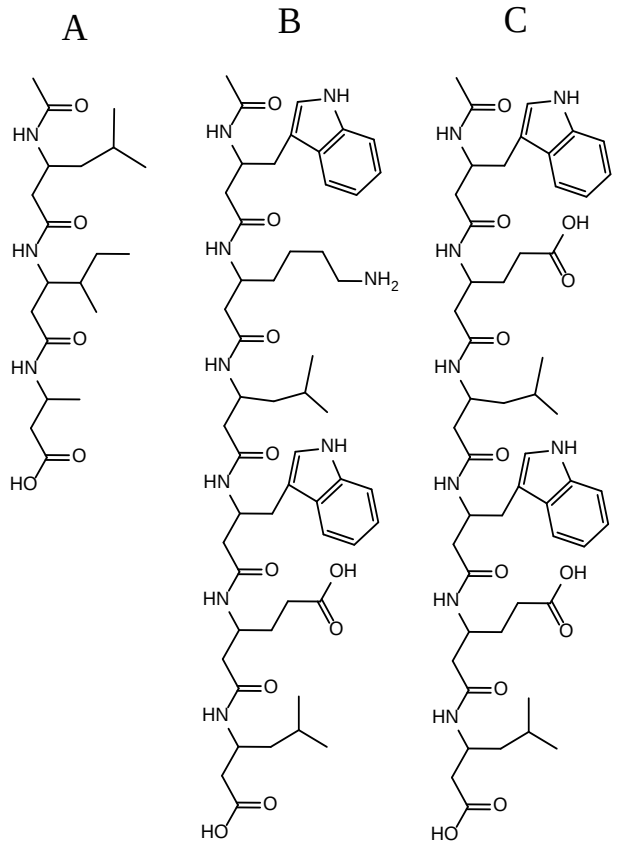

Figure 2. Chemical stuctures of (A) Ac-β^3[LIA], (B) Ac-β^3[WKLWEL] and (C) Ac-β^3[WELWEL]

Materials and Methods

Materials

Three substituted oligoamides, Ac-β^3[LIA], Ac-β^3[WELWEL], and Ac-β^3[WKLWEL] (Fig.2) were prepared using standard solid phase fmoc peptide synthesis on Wang resin as described previously, and acylated post synthesis but proir to resin cleavage [15]. Materials were HPLC purified using a preparative monolythic Onyx C18 column. For all experiments peptide solutions were created based on measured weight of lyophilized

peptides. Prior evidence suggests that the peptides assemble under all conditions and in all solvents, including acetone and DMSO, forming a colloidal system of very large fibres, some of which might have pre-existed in the solid, and the appearance of these fibres does not alter with dilutions within a wide range; surface deposits can be washed with excess solvent without removing the fibres[13, 17, 18]. Therefore the suspensions were used as is and concentrations are not measured more precisely. Considering that the samples were chemically synthesized and purified, and that suspensions of large fibres are known to form readily under these conditions there was no need for filtration or centrifugation prior to the scattering experiments.

Small angle neutron scattering (SANS)

All measurements were performed on the SANS (QUOKKA) instrument at the Australian Nuclear Science and Technology Organization at Lucas Heights, NSW, Australia. The substituted oligoamides were prepared to the highest dissolvable concentration achievable in deuterated water, resulting in approximate concentrations of 1 X 10^{-2} M (Ac-β^3[LIA]), 2.00 X 10^{-3} M (Ac-β^3[WELWEL]), and 3 X 10^{-3} M (Ac-β^3[WKLWEL]). 30% deuterated ethanol (v/v) was added to the Ac-β^3[LIA] sample to reduce hydrophobic attraction between fibres and thus promote dispersion of very large aggregates, as previous attempts showed no scattering when large aggregates of material where present, which causes sample to sediment out of the beam path. Samples were left in incubator (40°C) overnight to aid dissolution. Scattering profiles of each sample were collected to 7200 counts using 2 mm path length cylindrical Hellma cells. For stepwise temperature ramping 30-minute equilibrium times at each temperature before measurements commenced, at 25°C, 50°C, 70°C, 80°C. Samples were cooled to 25°C and measured as described above to determine any permanent morphological changes due to temperature.

Isotropic scattering patterns were collected at two sample to detector distances, 2 m (count time 10 minutes) and 14 m (count time 2 hours) with neutrons of 5 Å wavelength ($\boldsymbol{\lambda}$), with a variance of $\Delta\boldsymbol{\lambda}/\boldsymbol{\lambda}$ = 10%. The data was reduced to a 2-dimensional scattering pattern of intensity vs the scattering form I(q), using a cell filled with D_2O for Ac-β^3[WKLWEL] and Ac-β^3-[WELWEL] and D_2O + 30% EtOD for Ac-β^3-[LIA] in the ANSTO SANS macros ([24]) for IgorPro6 (Wavemetric, Oswego, USA) (REF).

An elliptical cylindrical model fitting (eq.I) was applied in Sasview fitting software (http://www.sasview.org/), based on previous information about common morpholigical shapes of the substituted oligamides [20, 21], with the assumpion that the scattering is dominated by the form factor due to the dilute sample solutions; that is, that scattering is due to the morhpological envelope of the suspended sample.

$$I(q) = \left(\frac{scale}{Vcyl}\right) \int d\psi \int d\phi \int p(\theta, \phi, \psi) F2(q, \alpha, \psi) sin\theta d\theta \; + \; background \qquad \text{(eq.I)}$$

Where:

scale is the volume fraction

V_{cyl} is the volume of the cylinder

ψ is the rotation about the cylinder axis

ϕ is the rotation about the beam

θ is the axis to beam angle

$$F(q, \alpha, \psi) = \frac{2J_1(a)}{a} . \frac{sin(b)}{b}$$

$$a \; = \; q . sin\,(\alpha)[r2majorsin2(\psi) \; + \; r2minorcos\,(\psi)]^{\frac{1}{2}}$$

$$b \; = \frac{qL}{2}(\alpha)$$

and *background* is the source background

In the modelling scattering length densities and the dimensions of the structures were constrained within boundaries defined by known information about the oligomades, to optimise the fit. Scattering length densities were calculated for each oligoamide in IgorPro7 software with the Irena SAS macrose[25]. The partial molar values required for these calucalations were determined using the CRYSOL method [26], using PDB files of similar oligamides generated experimantaly that were side-chain modifed in Chimera [27] to accurately represent each oligoamide. The SLD values for the background were also constrained. This value for the D_2O +30% EtOD background used for Ac-β^3-[LIA] was caluculated with Irena SAS macros [25] in IgorPro7, with a density that was aprroximated by the molar ratios of D_2O to EtOD in the solution (eq.II)

$$D_{D_2O+30\%\,EtOD} = \frac{1}{\left(\frac{n_{D_2O}}{n_{D_2O+30\%\,EtOD}} \times \frac{1}{D_{D_2O}}\right) + \left(\frac{n_{EtOD}}{n_{D_2O+30\%\,EtOD}} \times \frac{1}{D_{EtOD}}\right)} \quad \text{(eq.II)}$$

Where:

$D_{D_2O+30\%\,EtOD}$ is the density of D_2O +30% EtOD

n_{D_2O} is the number of mols of D_2O

n_{EtOD} is the number of mols of EtOD

$n_{D_2O+30\%\,EtOD}$ is the number of mols of D_2O +30% EtOD

$D_{D_2O}$is the denisty of D_2O

D_{EtOD} is the density of EtOD

Plots of the 2-dimensional data and model fits presented in Table 1 were prepared in Origin(Pro) software

Dynamic light scattering (DLS)

The oligoamide was dissolved in H_2O to a concentration of 2. X 10^{-3} M and aged for 20 days. Measurements were performed with a Malvern ZetasizerNano instrument (Malvern Instruments, Malvern UK) in a 1 cm quartz cuvette, at with a detection angle of 173°. A temperature ramping program was used to obtain measurements at 25°C, 50°C, 70°C, 80°C, and then returned to 25°C, with at least ten minutes equilibrium time between each step. A minimum of three measurements were taken for each temperature step, with each measurement consisting of multiple scans optimized by the software for sufficient signal to noise ratio for a reliable fit. Particle diameters were found using the narrow multiple modes fitting tool with Non Negative Least Squares method of the Malvern software. Error is provided as the cumulant polydispersity index (PdI). Peak sizes and PdI value were averaged across all measurements at each temperature step to give final values. Plots presented in Table 2 were prepared in OriginPro software (OriginLab).

NMR

Ac-β^{-3}-[LIA] was dissolved in 5% D_2O/H_2O to a concentration of approx 3 X 10^{-6} M. During this process, the sample was heated to 50°C to aid dissolution. NMR spectra were acquired on a Bruker spectrometer at 500Mz. The temperature dependence of the spectra was determined by acquiring 1D ^{1}H NMR data at 25°C, 50°C, 70°C, 80°C. Spectra were referenced

according to Wishart et al[28]. The reversibility of the temperature changes was determined by allowing the sample to cool to 25°C from 80°C and left for 24hrs before taking a final NMR measurement. Chemical shift assignments and coupling constants were determined from a 1D 1H NMR spectrum and 2D $^{1}H,^{13}C$ HSQC, ^{1}H-TOCSY with an 80 ms mixing time and ^{1}H DQF COSY spectra and tabulated in Table NMR1. In addition, a NOESY (600 ms mixing time) and ROESY (400 and 800 ms mixing times) spectra with were acquired. A self-diffusion measurement was performed at 298 K using a stimulated echo pulse sequence with bipolar gradient pulses provided in the standard Bruker pulse program library. The diffusion spectra were analysed in Topspin (Bruker AG). The hydrodynamic radius was estimated from the experimentally determined diffusion constant using the program SEGWE with the Stokes-Einstein-Gierer-Wirtz method [29].

Infrared Spectroscpy

All IR-spectroscopy measurements were performed at the IRIS beamline at the BESSY(II) storage ring at Helmholtz Zentrum, Berlin (HZB). The Ac-β^3[LIA] oligoamide was dissolved in isopropyl alcohol and deposited onto a 0.5 mm thick ZnSe disc and dried under ambient conditions. Data was collected on a gas purged Nicolet Continuμm Infrared Microscope (Thermo Scientific) linked to a Nexus 870 FT-IR spectrometer using Cassegrain infrared reflective objectives using OMNIC Atlμs software. Temperature was controlled by a Linkam stage cell, with controlled cooling achieved with liquid nitrogen. Measurements were taken at -180°C, -10°C, 25°C, 50°C, and 80°C. Each sample measurement was collected to 128 scans with a 4 cm^{-1} resolution and a 15 x 15 μm synchrotron source illumination area set by a knife edge aperture. Backgrounds measurements were collected to 256 counts using a nearby clean area of the ZnSe disc. Data was exported into OriginPro software to prepare the plots presented in Fig. 6.

Atomic force microscopy (AFM)

A solution of Ac-β^3[LIA] was prepared to a concentration of 2 X 10^{-3} M in H_2O and aged for 1 week. 1 μl of the solution was deposited on freshly cleaved mica and allowed to dry overnight at ambient temperatures and imaged the following day. The remaining solution was heated to 80°C for 4 hrs. Three 1 μl deposits were prepared from the 80°C solutions onto freshly cleaved micra, to by dried under different conditions. One sample was instant

dried by blowing argon gas over the sample for 15 minutes, and immediately imaged using AFM. A second sample was dried in at 80°C overnight and imaged the following day. A third sample was dried overnight under ambient conditions and imaged the next day. This sample was left at ambient conditions for another week, and re-imaged to determine whether any morphological changes occurred over this period in the solid phase.

All imaging was performed in semi contact mode on a Ntegra AFM platform and software (NT-MDT, Zelenograd, Russia), using silicone probes with 140-390 kHz resonance frequencies (force constant of 3-37 N/nm). Gwyddion software (www.gwyddion.net, Czech Metrology Institute), was used for all data processing.

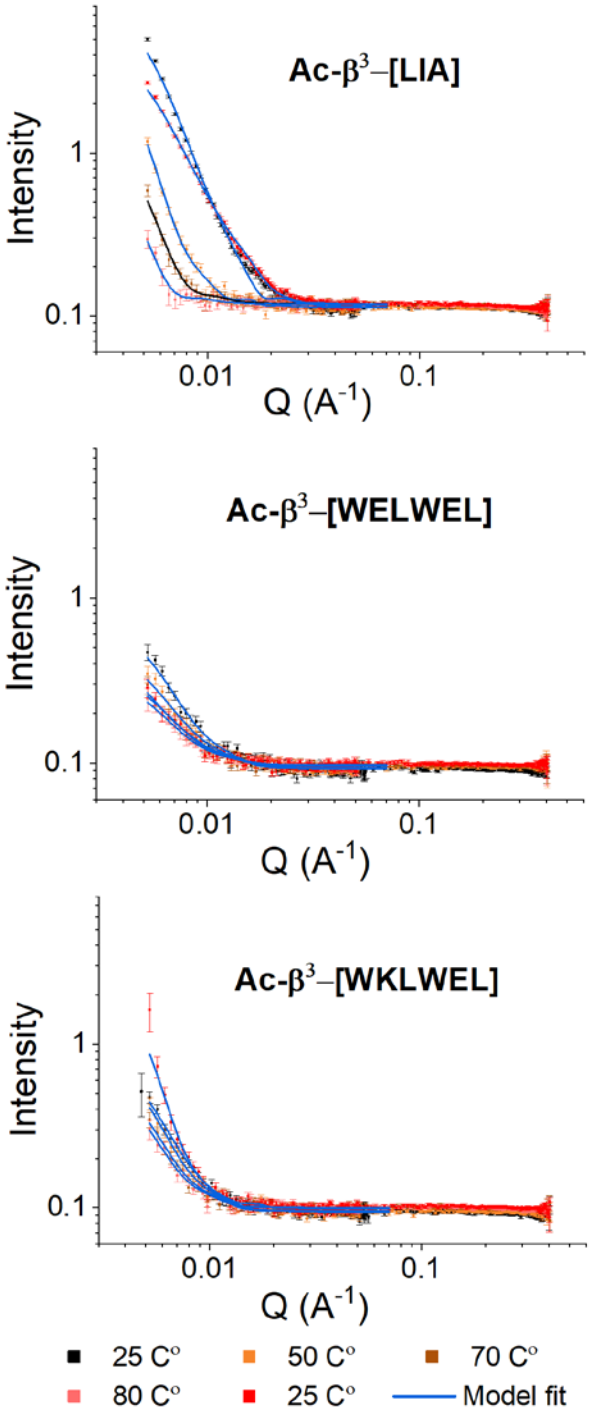

Figure 3. Fitted SANS data on Ac-β³[LIA], Ac-β³[WELWEL], and Ac-β³[WKLWEL] structrues present in solution

Results and discussion

SANS

SANS measurements of the samples give information on the average morphological envelope of the hydrogen-shell of each species within the solvent, in the Q-range of 0.004-0.4 (Fig. 3) . Due to the polydispersity of the oligoamide suspensions and the averaging nature of SANS measurements, this method can be used to identify overall changes within a dynamic self-assembled system, rather than specific dimensions. Given the low information content nature of SANS, in

these measurements two six-residue oligoamides were used as reference, the scattering properties of which have been established before [20, 21]

SANS measurements of Ac-β^3[LIA] showed visible changes due to temperature. Fitting each scattering curve with an elliptical cylinder model [30] provides information of the morphological cross section of fibrous structures present in solution. The length parameters are less reliable due to the head-to-tail assembly motif of the oligoamides, where length is expected to be largely variable in any given sample, giving a very broad scattering pattern, exacerbated by the potential of the fibres to bend and the low scattering profile offered by the termini of the very thin fibres. Also given the documented propensity of the system to form very long fibres suggests that a population of the fibres may have lengths exceeding the Q range of the measurement.

Results of the elliptical model fitting (Table 1) show that the morphological cross section of Ac-β^3[LIA] is clearly temperature dependent. Starting from structures of 18.69 nm x 56.43 nm at 25°C, heating causes an *increase* to 33.32 nm x 229.59 nm at 50°C and 34.68 nm x 257.96 nm at 70°C, evolving into more symmetrical structures at 80° C with the main radii of 41.82 nm and 56.96 nm. Yet, returning the sample to 25°C reverses the process, yielding elliptical fibres of 11.98 nm x 56.70 nm main radii that are, within the conditions of a dynamic polydisperse system, nearly identical to the dimensions before heating. Thus the change is reversible as expected for a dynamic equilibrium, yet it manifests in apparently increasing size. The reversibility excludes temperature-triggered (activation energy-limited) self-

Table 1. Parameters of elliptical cylindrical model fitting applied to SANS scattering cuvres in figure 3

Sample	Temp	Radius Minor (nm)	Radius Major (nm)	Length (nm)
Ac-β^3[LIA]	25°C	18.69 ± 0.18	56.43 ± 3.43	71.23 ± 1.11
	50°C	33.89 ± 1.17	66.78 ± 6.18	263.06 ± 12.17
	70°C	37.83 ± 2.24	67.69 ± 9.99	275.73 ± 21.05
	80°C	41.82 ±6.08	56.96 ± 25.24	112.35 ± 22.91
	25°C	11.98 ± 0.13	56.70 ± 4.78	65.08 ± 1.21
Ac-β^3[WELWEL]	25°C	15.80 ± 1.03	44.74 ± 14.01	121.55 ± 22.13
	50°C	13.11 ± 1.15	43.69 ± 15.58	136.54 ± 30.96
	70°C	13.87 ± 1.33	49.09 ± 24.93	154.03 ± 45.10
	80°C	14.34 ± 2.09	45.95 ± 27.74	142.72 ± 51.49
	25°C	13.99 ± 1.56	43.02 ± 20.00	133.03 ± 40.76
Ac-β^3[WKLWEL]	25°C	19.48 ± 1.23	63.97 ± 28.55	74.20 ± 8.06
	50°C	21.10 ± 1.36	50.99 ± 18.37	91.78 ± 16.97
	70°C	21.52 ± 1.93	52.93 ± 30.46	92.13 ± 26.15
	80°C	21.92 ± 2.38	52.92 ± 31.59	95.38 ± 28.24
	25°C	31.92 ± 2.09	68.52 ± 14.56	92.02 ± 5.17

assembly, therefore the most likely explanation is that the results are not related to the overall self-assembly equilibrium between monomers and fibres, rather it is a gradual loosening and therefore swelling of the fibre bundles described before [17] that at 80°C separate to thinner, more flexible fibres that roll up into “threadballs” but stiffen, therefore straighten and bundle again upon cooling.

The two larger oligoamides do not display a similar temperature trend, most likely due to the increased stability imposed on the structure by the greater number of H-bonding pairs compared to the tri-amide. Ac-β^3 [WELWEL] shows high stability with structures consistently within the range of 13.11 – 15.80 nm x 43.02 – 49.09 nm across all temperatures. The oligoamide Ac-β^3[WKLWEL] shows small changes with temperature; initial structures are 19.48 nm x 63.97 nm x74.20 nm at 25° C, which decrease in diameter and increase in length at 50° C, 70° C and 80° C (approx. 21 nm x 52 nm x 92 nm). Upon cooling, the minor radius shrinks back to 21.52 nm, however the length value remains increased. This shows remarkable robustness of the supramolecular structure formed by the hexa-amides and implies that the self-assembly equilibrium strongly favours the fibrous form for all three materials in the observed temperature range. It is important to note that the SANS measurements did not show any smaller structures for either of the samples, the data only contained noise in the Q range corresponding to the monomers. The data establishes the dominance of the fibrous form over aggregation but also confirms the anomalous behaviour of Ac-β^3[LIA] compared to the two hexa-amides and thus the self-assembly of this oligoamide is examined in further detail.

DLS

While SANS was used to extract the cross-sectional geometry of the fibres, DLS can measure hydrodynamic radii of tumbling structures up to micron range. DLS intensity scales with 10^{-6} of the radius of a particle, thus populations of larger structures dominate the measurements. It can detect a population of small species next to large aggregates if the smaller species is in a substantial excess, since scattering intensity scales with the 6^{th} power of the particle diameter. For this reason, and because the measurement yields hydrodynamic radii, DLS can be used principally to find any regularity in the lengths of the suspended structures, that cannot be reliably fitted in SANS, as a function of temperature.

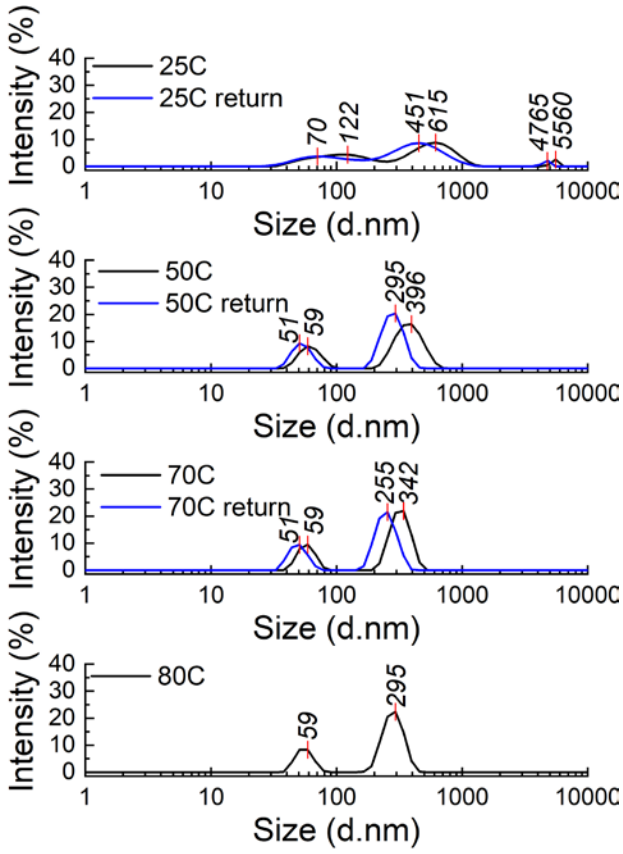

Figure 4. DLS data of Ac-β[3][LIA] structrues present in water at changing temperatures.

Table 2 DLS data in Ac-β[3]-[LIA] during temperature ramping (↑) and temperature cooldown (↓)

Temp	Peak 1 size	Peak 2 size	Peak 3 size	PdI
25° C ↑	560.03	97.14	3640.33	0.66
50° C ↑	383.48	61.86	-	0.37
70° C ↑	324.22	67.70	-	0.33
80° C	285.55	55.60	-	0.41
70° C ↓	290.62	57.34	-	0.50
50° C ↓	327.31	61.55	-	0.38
25° C ↓	525.23	91.90	5428.333	0.75

Measurements on Ac-β[3][LIA] in water under changing temperatures show clear changes with temperature (Table 2). Large aggregate structures, nominally around 3640 nm diameter but likely highly polydisperse, are clearly present in the sample at 25° C and disappear when the temperature is increased to 50° C. This implies that they were caused by nonspecific (weakly associated) aggregation. Two smaller populations, with initial diameters of 122nm and 615 nm, reduce in overall size to 59 nm and 295 nm, respectively, when heated to 80°C, with noticeably narrowing size distributions (table 2). The trend is reversed upon complete cooling. The DLS data confirms that the overall sizes, i.e. lengths of the structures do decrease, with the smaller population corresponding reasonably well to the major radii in the SANS data, suggesting that there is a population of smaller ellipsoid structures of specific dimensions that in SANS overlap with the long fibres of the same cross section. The loose agreement between the second DLS population to the lengths of the elliptical cylinders in SANS, i.e. the presence of a more elongated population alongside the ellipsoidal one further confirms this interpretation. Due to the partial overlap of dimensions these two populations could

not be clearly resolved in SANS.

NMR

NMR was used to detect the small species that were not identifiable in the scattering experiments. Temperature effects on the NMR spectra of were examined on a 5% $^{2}H_2O$ solution of Ac-β^{-3} [LIA].

The linewidths and experimentally determined diffusion constant that falls in the range 3.44-6.23 $\times$ 10^{-10} m^2 s^{-1}. (~3.98 $\pm$ 0.03 $\times$ 10^{-10} m^2 s^{-1} at 298K) (Table 3) are indicative of monomeric or possibly a dimeric species under the conditions that the NMR spectra where acquired. Both the linewidths and the observation of positive NOEs of all samples in the NOESY spectrum are consistent with a low molecular weight species. The positive NOE values implies that the rotational correlation, τ_c, time is smaller than 1.12/ω where ω is the spectrometer frequency, i.e.

Table 3. Ac-β^{-3}[LIA] chemical shift and J coupling constants[a] under aqueous conditions

residue	**$^{3}J_{HNH\alpha}$ /Hz**		**chemical shift /ppm**
Ac		$\delta^{1}H$	CH_3, 1.98
		$\delta^{13}C$	CH_3, 24.8
Leu1	9.2	$\delta^{1}H$	HN, 7.88; HA, 4.19; HB1, HB2, 1.44, 1.29;HG1, 1.61;QD1,QD2 0.91, 0.88; HB21, HB22, 2.42, 2.36
		$\delta^{13}C$	CA 48.6; CB 45.7; CG 27.1; CD1, 25.2; CD2 23.8; CB2 44.7
Ile2	9.7	$\delta^{1}H$	HN, 7.92; HA 4.08; HB, 1.54; HG11, HG12, 1.45, 1.11 ; QG2 0.89; QD1 0.90; HB21, HB22 2.50, 2.27
		$\delta^{13}C$	CA 54.4; CB 40.8; CG1 27.4; CG2 17.3; CD1, 13.5; CB2 40.8
Ala3	8.5	$\delta^{1}H$	HN, 7.96; HA 4.20; QB, 1.18; QB2 2.49
		$\delta^{13}C$	CA 45.8; QB 22.0; CB2 44.2

[a]resonances are named according to standard α-amino acid conventions. The side chain bearing carbon CA and attached proton HA, the stereospecific resonance assignment was not performed.

$$\tau_c < 2.24 \times 10^{-9} s \quad \text{(eq.III)}$$

where the NOE has zero intensity [31]. Using the Debye equation and the hydrodynamic radius, r_H, determined from the diffusion measurement.

$$\tau_c = \frac{4\pi\eta r_H^3}{3kT} \quad \text{(eq.IV)}$$

$$r_H = 739 \times 10^{-12} m \quad \text{(eq.V)}$$

Where:

η is viscosity, with a value of 0.8921 mPa s

k is the Boltzmann constant with a value of 1.380649×10^{-23} J·K^{-1}

T is Temperature with a value of 298K

From the hydrodynamic radius determined from the experimental diffusion constant

$$\tau_c \sim 3.7 \times 10^{-10} s \quad \text{(eq.VI)}$$

Thus, these NOESY data predict a hydrodynamic radius in the range of 603-983 pm dominated by a species of 739 pm that, based on average density of peptides, is consistent with a molecular mass in the range of 347-1502 Da, with the dominance of a 638 Da species.

Combined, the linewidth and NOESY data indicate a low molecular weight species in solution for Ac-β^3[LIA] under the conditions that NMR spectra were acquired, consistent with small peptides[32, 33] . The JHNHα coupling constants are all ≥8.5 Hz consistent with a dihedral angle of ~120 deg that is normally interpreted as an extended structure.

A simple and valuable experiment to determine the presence of hydrogen bonding network among amide protons is to examine the temperature dependence of the amide proton resonance[34]. The amide proton temperature dependency ($\Delta\delta(HN)/\Delta T$) is a strong predictor of the presence of a hydrogen bond. Amide protons with a temperature coefficient more positive than -4.6 ppb/K are strongly predicted to be participating in a hydrogen bond[34]. Under the conditions of the spectral acquisition of Ac-β^3[LIA] all amides had temperature coefficients more negative than -4.6 ppb (Fig. 5) and this implies the absence of any hydrogen bonded oligomeric species. The chemical shift behaviour was reversible and on cooling the resonances return to their original positions in the spectrum and there were no obvious changes in resonance intensity on heating the sample. These indicate the reversibility and the behaviour as a monomeric species at all temperatures. There were no obvious temperature dependent intensity differences indicating aggregation at higher temperatures, however, exchange broadening of the HN resonances occurs at the highest temperatures.

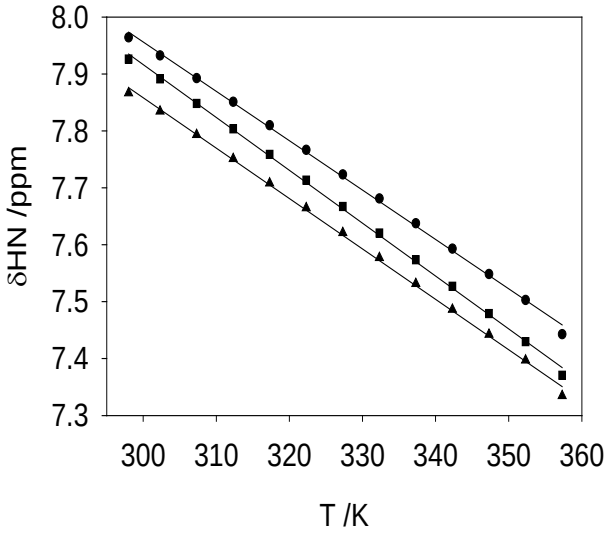

Figure 5. Amide chemical shift temperature dependence. Plot of the amide chemical shift (δHN) of Ac-β^{-3}-[LIA] against temperature. L1 triangles, I2 squares, A3 circles. The temperature coefficients are -8.85, -9.29 and -8.67 ppb/K for L1, I2 and A3 amide resonances respectively. All curves have a correlation coefficient (R^2) ≥ 0.999. Above 360 K the amide exchange rate moved into intermediate exchange broadening of the resonances making them difficult to assign.

Mid-IR

Mid-IR spectroscopy of Ac-β^3[LIA] in the solid state under humid conditions show very little change with temperature (Fig. 6). Most noticeable are the amide I and II bands at 1648 and 1547 cm^{-1}, respectively, that show no change with temperature. The amide I and II bands are sensitive to the secondary structure in oligoamides and peptides, as Amide I corresponds to C=O stretch and Amide II is a combination of CN stretch and NH bending vibrations of the

amide backbone[35-37]. The peaks seen here are consistent with 14-helical or 14-helix-like assembly [20, 22, 23, 35, 38-40], and show no change with temperature. Peaks between 1000-1500 are CH vibrations from the oligoamide side chain s[36, 41, 42], and are also highly consistent at each temperature step, indicating a highly conserved folding of the Ac-β^3[LIA] monomers; this suggests that in solid phase there is no considerable monomeric population; without the constrains of the superstructure monomers would likely exhibit more conformational variability.

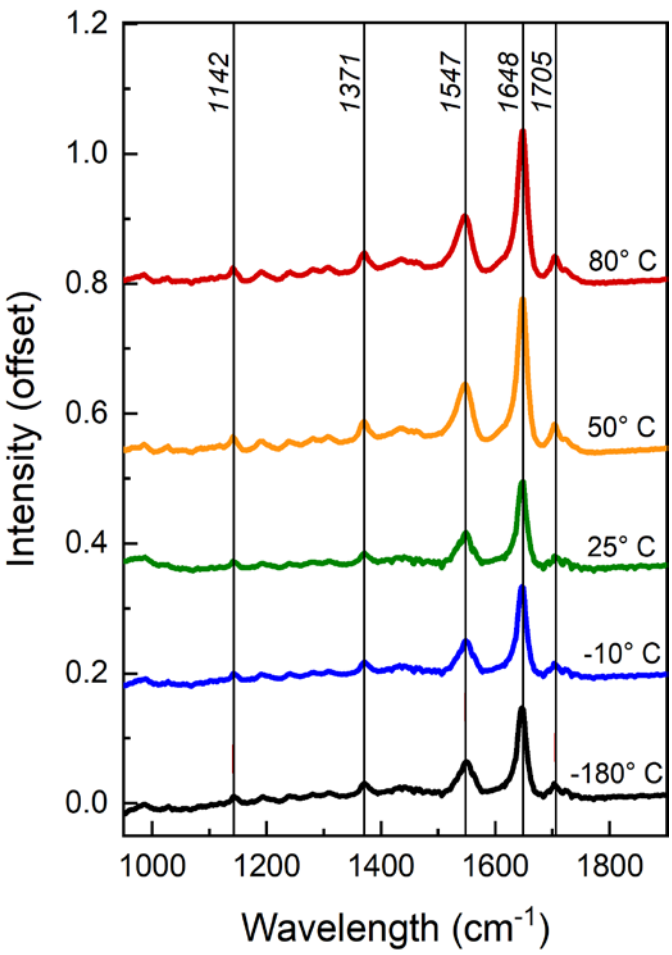

Figure 6. Mid-IR spectra of Ac-β^{-3}-[LIA] in the solid states at temperature ranging from -180° C to 80° C

AFM

AFM images of Ac-β^3[LIA] show the morphological structures present under dry conditions. Noting that the dry sample appears to be fully assembled according to previous AFM studies and vibration spectroscopy, while scattering experiments and NMR suggests apparently conflicting information about the state of the material in solution, AFM experiments were designed to examine this difference by comparing fast- and slow dried samples to confirm whether previously reported abundance of fibrous structures has formed during the drying process. When deposited from 80°C, and dried instantly (Figure 7A), the sample shows some fibrous structure of around 2-3 nm height but with lengths in the micron scale, confirming the observations of the scattering experiments. However, the deposit also contains islands of material underneath, consistent with a thin layer of amorphous mass of monomers. When deposited from 80° C solution and aged at 80° C overnight (Fig. 7B), further breakdown is apparent, with only small islands of amorphous material (approx. 2 nm)

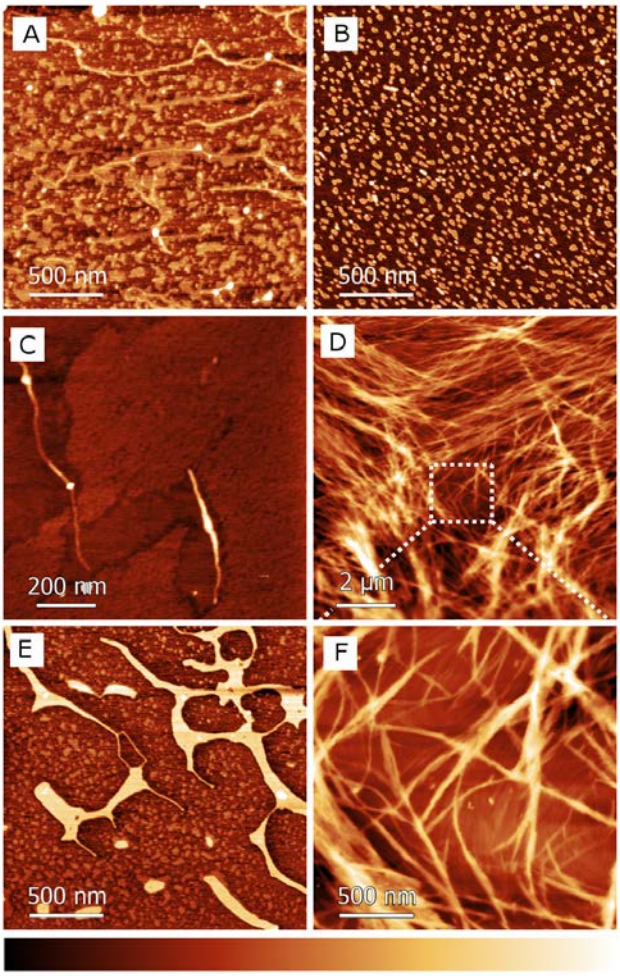

Figure. 7: Ac-β[3][LIA] (A) deposited 80C instant dry (B) deposited 80C and dried overnight at 80C (C) deposited 80C, dried overnight at 25C (D) Sample C after one week at room temperature; (F) is a zoom into (D). (E) deposited 25C and dried over-night 25C. Colour scale gives structural height (A) 3.2 nm (B) 2.6 nm (C) 2.4 nm (D) 132.8 (E) 6.2 nm (F) 66.3 nm.

present. When deposited at 80° C but dried at 25 ° C overnight (Fig. 7C), the scattered islands visible in (Fig. 7B) appear to have arranged into a more organized background layer, with a few visible fibres of 1-2 nm over the top. Deposition from 25°C and dying at 25°C overnight (Fig. 7 E) appears similar but with more fibrous material assembled into taller island on top of the amorphous background layer, suggesting that there are larger fibrous assemblies in solution, or a regular size, consistent with the scattering experiments. After aging the sample in Figure 4C under dry ambient conditions for 1 week, rescanning the sample revealed a multitude of fibres present (Fig. 7D and F), with a total disappearance of amorphous material, indicating that the material can assemble under dry conditions. This suggests that pure monomeric Ac-β[3][LIA] is a viscous fluid at room temperature, consistent with the lack of any intermolecular hydrogen bonding, but specific assembly into fibres yields a solid.

Discussion

According to the experimental data for solution phase measurements, Ac-β[3][LIA] exists in either very large fibrous assemblies or in monomeric state without any intermediate oligomers; this was confirmed by AFM imaging comparing fast dried and slow dried deposits, the former showing the co-existence of micrometer size fibrous and amorphous, likely

monomeric states. Aging the dry deposits at room temperature for extended time however yielded an almost exclusively fibrous material as confirmed with AFM and IR spectroscopy. Solid state self-assembly was also noted before in case of deposits from isopropanol[17] but has not been observed for deposits from water.

It is important to emphasize that in all cases either very large assemblies are detected (>0.5 GDa based on the volume and known density of the peptide) or monomeric/amorphous material, whereas any intermediate structures, small oligomers or core nanorods are absent. Hence, the experiments clearly show that the samples contain a substantial population of large superstructures (seen *via* SANS, AFM and DLS) with a large excess of monomers, which is seen *via* NMR. The fact that the IR reveals highly structured materials, and that the AFM shows a transformation of amorphous deposit to fibrous material in solid state suggests that a dynamic equilibrium between the fibrous and monomeric form is possible, it is however inhibited in aqueous solution.

The overall thermal stability of the assemblies parallel with the abundance of monomers but in a total absence of small oligomers in solution leads to two key conclusions. One, the monomer to monomer binding energy of the hydrogen bond motif of the Ac-β^3[LIA] in the fibrous assemblies well exceeds kT in the studied temperature range, which is only possible if the three hydrogen bonds (Fig. 1) facilitating the self-assembly are shielded from the high dielectric environment of, and direct competition for amide hydrogen bonding sites by water. That is, strength of hydrogen bonding is not much weakened compared to its gas phase theoretical maximum. This is consistent with former observations showing that Ac-β^3[LIA] can form fibres in highly polar solvents such as acetone and DMSO [13, 16-18]. Thus the fibres remain intact and all observed changes in size are related to the lateral bundling between the fibres, and potential changes in flexibility and resulting rolling into more spherical “threadball” structures.

The second important observation is the apparent inability of the monomers in aqueous solution to either join an existing fibre, or nucleate a new one. The only feasible explanation of this phenomenon is the existence of a substantial energy barrier for the monomers to join the three-point hydrogen bonding motif; that can only be a geometric mismatch. The JHNHα coupling constant of the NMR data suggests that the monomeric species are extended, which is only possible in a conformation where the side chains are on opposing sides of the

oligoamide backbone. According to the literature β-amino acids can freely rotate at the C^2-C^3 bond (where carbons are numbered following peptide chemistry conventions) in the absence of substituents, whereas substitution at either beta carbon as in case of Ac-β^3[LIA] hinder this free rotation [2]. Assuming the existence of an extended and a loop conformer, where the side chains are on alternating sides or the same side, respectively, of the backbone, the extended form involves the inversion of the dipole of one or more amides, only allowing very weak hydrogen bonding between monomers as the backbone is in this case exposed to water at its full length. This explains the absence of even small nonspecific oligomers. This linear form cannot join the 14 helix-based self-assembly motif of the fibres and that explains the lack of spontaneous nucleation and lack of a dynamic equilibrium between monomers and the fibres. The data suggest that hydration stabilizes the extended conformer and thus the self-assembly is very slow unless the thermal motion of the molecule reaches this activation energy barrier. This is consistent with the observation that sometimes heating does induce extensive fibre growth of freshly dissolved lyophilized oligoamides [16].

The last point to note is the ability of the fibres to assemble in dry state, as seen through AFM (Fig. 7C &D). This is consistent with the notion that in aqueous solution hydration stabilizes the extended conformer, and thus in the absence of water monomers can change conformation within an observable timeframe. It also assumes that the monomeric oligoamides are in a fluid-like state that is consistent with the appearance of islands of thin layers in AFM images. Consistently, previously observed variations in solubility and self-assembly behaviour of Ac-β^3[LIA] are closely related to the lyophilization and storage conditions that may result in varying amounts of fibrous assembled and linear monomeric species where the latter may be conserved if cold stored. This is unique to the short sequence of Ac-β^3[LIA] in the absence of bulky side chains.

Conclusion

The self-assembly of Ac-β^3[LIA] was studied by using a comprehensive approach of scattering methods, NMR, AFM and IR. The results indicate that, while there is a monomeric population of Ac-β^3[LIA] in solution, small oligomers/short fibres are not detected, only very large, GDa range assemblies consistent with extensive bundling of Ac-β^3[LIA] nanorods. The absence of small

oligomers suggests that the self-assembly of Ac-β^3[LIA] is nucleation-limited, consistent with the existence of two conformers: a 14 helix-like, or "horseshoe" confirmation and an extended monomeric form, the first of which readily attaches to growing fibres while the second is prohibited geometrically from doing so. It is likely that hydration of the amide moieties of the carbon backbone stabilizes the extended form by blocking the 3-point hydrogen bonding motif between the N and O group of the amide moieties. Thus fibre growth might be triggered by conditions that allow increased conformational freedom of the monomer allowing greater control of these supramolecular assemblies potentially leading to applications in tissue scaffolding and high porosity nanostructured materials.

1. Seebach D, Matthews JL. beta-peptides: a surprise at every turn. Chem Commun. 1997(21):2015-22.
2. Cheng RP, Gellman SH, DeGrado WF. beta-peptides: From structure to function. Chem Rev. 2001;101(10):3219-32.
3. Gellman SH. Foldamers: A manifesto. Accounts Chem Res. 1998;31(4):173-80.
4. Seebach D, Overhand M, Kuhnle FNM, Martinoni B, Oberer L, Hommel U, et al. beta-peptides: Synthesis by Arndt-Eistert homologation with concomitant peptide coupling. Structure determination by NMR and CD spectroscopy and by X-ray crystallography. Helical secondary structure of a beta-hexapeptide in solution and its stability towards pepsin. Helv Chim Acta. 1996;79(4):913-41.
5. Abele S, Seiler P, Seebach D. Synthesis, crystal structures, and modelling of beta-oligopeptides consisting of 1-(aminomethyl)cyclopropanecarboxylic acid: Ribbon-type arrangement of eight-membered H-bonded rings. Helv Chim Acta. 1999;82(10):1559-71.
6. Horne WS, Gellman SH. Foldamers with Heterogeneous Backbones. Accounts Chem Res. 2008;41(10):1399-408.
7. Appella DH, Christianson LA, Klein DA, Richards MR, Powell DR, Gellman SH. Synthesis and structural characterization of helix-forming beta-peptides: trans-2-aminocyclopentanecarboxylic acid oligomers. J Am Chem Soc. 1999;121(33):7574-81.
8. Seebach D, Gademann K, Schreiber JV, Matthews JL, Hintermann T, Jaun B, et al. 'Mixed' beta-peptides: A unique helical secondary structure in solution. Helv Chim Acta. 1997;80(7):2033-8.
9. Raguse TL, Lai JR, LePlae PR, Gellman SH. Toward beta-peptide tertiary structure: Self-association of an amphiphilic 14-helix in aqueous solution. Org Lett. 2001;3(24):3963-6.
10. Appella DH, Christianson LA, Karle IL, Powell DR, Gellman SH. beta-peptide foldamers: Robust Helix formation in a new family of beta-amino acid oligomers. J Am Chem Soc. 1996;118(51):13071-2.
11. Raguse TL, Lai JR, Gellman SH. Environment-independent 14-helix formation in short beta-peptides: Striking a balance between shape control and functional diversity. J Am Chem Soc. 2003;125(19):5592-3.
12. Appella DH, Christianson LA, Klein DA, Powell DR, Huang XL, Barchi JJ, et al. Residue-based control of helix shape in beta-peptide oligomers. Nature. 1997;387(6631):381-4.
13. Seoudi RS, Hinds MG, Wilson DJD, Adda CG, Del Borgo M, Aguilar M-I, et al. Self-assembled nanomaterials based on beta (beta(3)) tetrapeptides. Nanotechnology. 2016;27(13).
14. Gopalan RD, Del Borgo MP, Mechler AI, Perlmutter P, Aguilar MI. Geometrically Precise Building Blocks: the Self-Assembly of beta-Peptides. Chem Biol. 2015;22(11):1417-23.
15. Del Borgo MP, Mechler AI, Traore D, Forsyth C, Wilce JA, Wilce MCJ, et al. Supramolecular Self-Assembly of N-Acetyl-Capped beta-Peptides Leads to Nano- to Macroscale Fiber Formation. Angew Chem-Int Edit. 2013;52(32):8266-70.

16. Seoudi RS, Dowd A, Smith BJ, Mechler A. Structural analysis of bioinspired nano materials with synchrotron far IR spectroscopy. Phys Chem Chem Phys. 2016;18(16):11467-73.
17. Seoudi RS, Dowd A, Del Borgo M, Kulkarni K, Perlmutter P, Aguilar MI, et al. Amino acid sequence controls the self-assembled superstructure morphology of N-acetylated tri-beta(3)-peptides. Pure Appl Chem. 2015;87(9-10):1021-8.
18. Seoudi RS, Del Borgo MP, Kulkarni K, Perlmutter P, Aguilar MI, Mechler A. Supramolecular self-assembly of 14-helical nanorods with tunable linear and dendritic hierarchical morphologies. New J Chem. 2015;39(5):3280-7.
19. Mechler A, Seoudi R, Del Borgo MP, Aguilar M-I, Perlmutter P. Nano-architecture: creating complex surface structures using supramolecular self-assembly of tripeptides. Micro/Nano Materials, Devices, and Systems. 2013;8923.
20. Buchanan C, Garvey CJ, Puskar L, Perlmutter P, Mechler A. Coordination crosslinking of helical substituted oligoamide nanorods with Cu(II). Supramolecular Chemistry. 2020;32(3):222-32.
21. Buchanan C, Garvey CJ, Perlmutter P, Mechler A. Co-assembly of helical beta(3)-peptides: a self-assembled analogue of a statistical copolymer. Pure Appl Chem. 2017;89(12):1809-16.
22. West NG, Seoudi RS, Barlow AJ, Qi DC, Puskar L, Del Borgo MP, et al. A two-dimensional metallosupramolecular framework design based on coordination crosslinking of helical oligoamide nanorods (vol 1, pg 1134, 2020). Mater Adv. 2020;1(9):3605-.
23. West NG, Seoudi RS, Barlow AJ, Qi DC, Puskar L, Del Borgo MP, et al. A two-dimensional metallosupramolecular framework design based on coordination crosslinking of helical oligoamide nanorods. Mater Adv. 2020;1(5):1134-41.
24. Kline SR. Reduction and analysis of SANS and USANS data using IGOR Pro. J Appl Crystallogr. 2006;39:895-900.
25. Ilavsky J, Jemian PR. Irena: tool suite for modeling and analysis of small-angle scattering. J Appl Crystallogr. 2009;42:347-53.
26. Svergun D, Barberato C, Koch MHJ. CRYSOL - A program to evaluate x-ray solution scattering of biological macromolecules from atomic coordinates. J Appl Crystallogr. 1995;28:768-73.
27. Pettersen EF, Goddard TD, Huang CC, Couch GS, Greenblatt DM, Meng EC, et al. UCSF chimera - A visualization system for exploratory research and analysis. J Comput Chem. 2004;25(13):1605-12.
28. Wishart DS, Bigam CG, Yao J, Abildgaard F, Dyson HJ, Oldfield E, et al. H-1, C-13 AND N-15 CHEMICAL-SHIFT REFERENCING IN BIOMOLECULAR NMR. J Biomol NMR. 1995;6(2):135-40.
29. Evans R, Dal Poggetto G, Nilsson M, Morris GA. Improving the Interpretation of Small Molecule Diffusion Coefficients. Anal Chem. 2018;90(6):3987-94.
30. Feigin LA, Svergun DI. Structure Analysis by Small-Angle X-ray and Neutron scattering. Taylor GW, editor. New York: Plenum; 1987.
31. Neuhaus D, Williamson M. The nuclear overhauser effect in structural and conformational analysis. J prakt Chem 1990;332(5):658-.
32. Pei HX, Germann MW, Allison SA. Translational Diffusion Constants of Short Peptides: Measurement by NMR and Their Use in Structural Studies of Peptides. J Phys Chem B. 2009;113(27):9326-9.
33. Danielsson J, Jarvet J, Damberg P, Graslund A. Translational diffusion measured by PFG-NMR on full length and fragments of the Alzheimer A beta(1-40) peptide. Determination of hydrodynamic radii of random coil peptides of varying length. Magnetic Resonance in Chemistry. 2002;40:S89-S97.
34. Cierpicki T, Otlewski J. Amide proton temperature coefficients as hydrogen bond indicators in proteins. J Biomol NMR. 2001;21(3):249-61.
35. Kong J, Yu S. Fourier transform infrared spectroscopic analysis of protein secondary structures. Acta Biochim Biophys Sin. 2007;39(8):549-59.
36. Barth A. Infrared spectroscopy of proteins. Biochim Biophys Acta, Bioenerg. 2007;1767(9):1073-101.
37. Barth A, Zscherp C. What vibrations tell us about proteins. Q Rev Biophys. 2002;35(4):369-430.

38. Vasantha B, Yamanappa H, Raghothama S, Balaram P. Conformational properties and aggregation of homo-oligomeric beta(3)(R)-valine peptides in organic solvents. Biopolymers. 2017;108(3).
39. Dutot L, Gaucher A, Elkassimi K, Drapeau J, Wakselman M, Mazaleyrat J-P, et al. Synthesis and characterisation of helical beta-peptide architectures that contain (S)-beta(3)-HDOPA (crown ether) derivatives. Chem: Eur J. 2008;14(10):3154-63.
40. Jansen TL, Dijkstra AG, Watson TM, Hirst JD, Knoester J. Modeling the amide I bands of small peptides. J Chem Phys. 2006;125(4):9.
41. Wolpert M, Hellwig P. Infrared spectra and molar absorption coefficients of the 20 alpha amino acids in aqueous solutions in the spectral range from 1800 to 500 cm(-1). Spectrochim Acta A. 2006;64(4):987-1001.
42. Barth A. The infrared absorption of amino acid side chains. Prog Biophys Mol Bio. 2000;74(3-5):141-73.